the continental crust, a much-processed material compared to the previous planetary examples, is not basaltic and requires considerable ingenuity and persistence to understand its petrogenetic processes and its growth in time. The mechanics of spreading ridges, trenches, and subduction zones are key aspects of the plate tectonic revolution of the past 50 years that make possible the understanding in outline of how planetary differentiation works at present and has worked for some portion of the Earth's past (Wyllie, 1973). It is not clear that the Earth has always worked in this way, but unlike the previous planetary examples surveyed, the initial differentiation and continuing early operation of Earth's evolution is poorly recorded because so much has been overwritten by the ongoing activity.

The escape of heat from Earth's interior drives the convective overturn of the interior. Temperature excesses create buoyant forces that promote convective movements so as to relieve temperature imbalances. Sinking of cool material from the surface and the rise of hot materials from depth are partly organized around the architecture of the semi-rigid tectonic plates capping the Earth's surface which derive their lateral motions from the vertical buoyant flows. It is thought that the sinking flows associated with convergent plate margins are more effective at moving the plates than the rising flows associated with divergent plate margins or with interplate plume flow (Davies and Richards, 1992). Nevertheless the passive upwelling curtain flows beneath divergent plate margins are responsible for generation of the most important flux of magma on the present Earth. This flux erupts as largely submarine mid-ocean-ridge basalt (MORB). The melting mechanism producing the MORB flux has been known in outline since Verhoogen (1954, 1973) elucidated decompression melting. The mechanism arises from the difference in P-T trajectory between the adiabatic decompression experienced by a parcel of warm, buoyant material rising from depth and the slope of a melting curve for the same material. For silicates of low thermal expansion, rock rising from depth too rapidly to exchange heat with the surroundings lowers its adiabatic temperature with decompression only slightly, on the order of 0.5 °C/km. This temperature drop is 3–6 times less than the decrease of the melting curves with falling pressure, so that a material starting off solid and compressed may in the process of decompressing begin to melt, crossing a steeper melting curve even as its temperature falls. Its temperature falls both because the adiabatic temperature falls with decompression and because the melting process requires energy and uses a further temperature fall to turn sensible heat of the solids into the latent heat of melting. The process has been analyzed in detail by McKenzie and Bickle (1988) with the compositional dimensions most thoroughly explored by Klein and Langmuir (1987) and Langmuir et al. (1992). The phase relations for MORB system melting have been fully explored by Kinzler and Grove (1992a, 1992b).

Early investigations of MORB emphasized their tholeiitic character, their lack of wide compositional dispersion, and their obviously low pressure partial crystallization (Fig. 6) (Muir et al. 1964; Engel and Engel, 1964; Engel et al., 1965; Miyashiro et al., 1969). Their emergence as a possible major rock type was in the context of the debate early in the time of our review period about so-called primary magmas. The concept of primary magmas arises in the context of the search for understanding the diversity of igneous rock types which are found in space and time. To Bowen (1928), using fractional crystallization to generate igneous lineages through cooling, a primary magma was one of sufficient abundance and wide enough distribution to plausibly give rise to a wider spectrum of derivative types. As his mechanism for diversifying eruptive products involved cooling, the primary material has to be supplied hotter than the derivatives. To the basalt mavens of the 1960 and 1970s (Yoder and Tilley, 1962; Cohen et al., 1967; DH Green and Ringwood, 1967a; O'Hara 1968a, 1968b; Presnall et al., 1979), the issues were a bit more complex. High eruption temperature and widespread abundance were no longer the only determinants of candidacy for primary status. The compositional details of the many variants of the types presented also had to be accommodated. The experimental details of which phases' crystallization and in which order

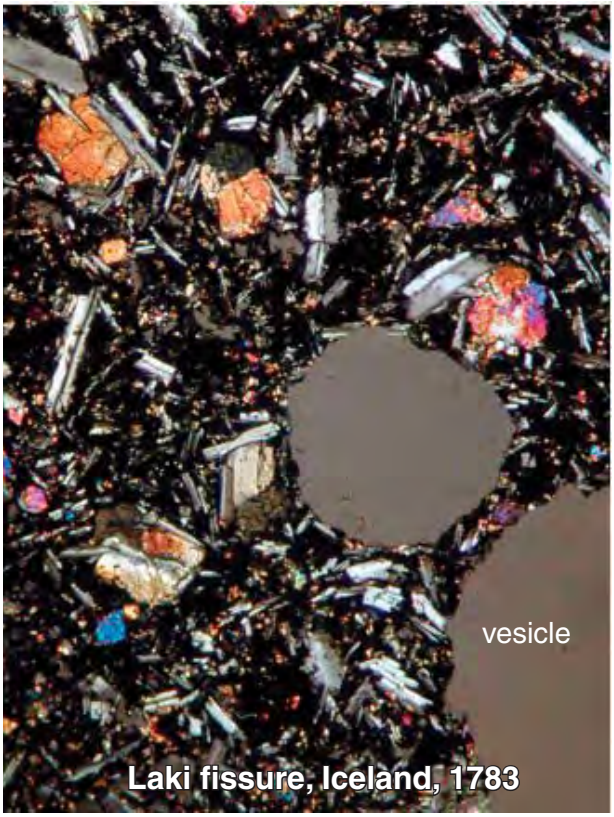

Figure 6. Photomicrograph in crossed nicols of vesicular tholeiitic basalt erupted from the Laki fissure, Iceland, in 1783. Plagioclase, olivine, and augite microphenocrysts are all present, whereas orthopyroxene is not. Aerosols and gas from this eruption had a considerable impact on the climate of the northern hemisphere, producing a virtually summerless year. Fortunately, most MORB tholeiites discharge under water. Horizontal dimension of the image is 5 mm.

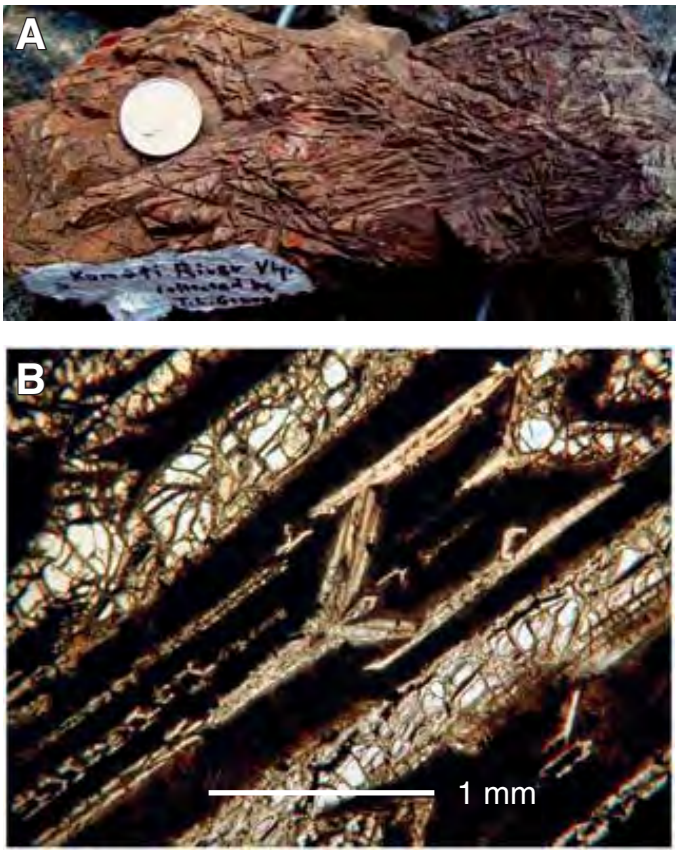

Figure 7. Komatiite: (A) hand specimen and (B) thin section. (A) Olivine plates intersecting the specimen's surface give characteristic spinifex texture. Hand specimen from Komatii River Valley, Barberton Mt. Land, S. Africa, courtesy of TL Grove. Dime for scale. (B) Thin section, plane-polarized illumination, of spinifex olivines in komatiite from Pike's Hill, Munro Twp., Ontario.

water content is responsible. But we have no completely faithful modern analogs for this rock association, reinforcing the suggestion that the Earth's tectonic past was different (Hamilton, 1998; Bédard et al., 2003). The prevalence of tonalite and trondjhemite granitoid lithologies in the Archean, in contrast to the increasing abundance of K-rich granites subsequently, shows up in the compositions of sediments derived from the respective source terranes with time. The observation of increasing K/Na in the sedimentary record is important to the McLennan and Taylor (1991) model of continental growth and again suggests that our geological past was different from the present.

The fourth line of evidence is that there appears to have been a qualitative change in Earth's surface atmospheric conditions near the Archean to Proterozoic boundary (Holland, 1984, 2002). Progressive oxygenation of the atmosphere, perhaps as a response to the rise of photosynthetic organisms, became apparent in the sedimentary rock record of the Proterozoic (Farquhar et al., 2000, 2010). The great oxygenation event has been recently been recognized as a turning point in the mineralogical evolution of our planet (Hazen et al., 2008, 2011; Hazen and Ferry, 2010). In the presence of an oxygenated atmosphere, minerals can form that were previously unstable in neutral or reducing atmospheres. Thus, bursts of new mineral species appear in the geological record. In like manner, new mineralogy develops in synchronization with the supercontinent-assembling episodes of the past. It is not a stretch to imagine that these changes could also rebound into the internal workings of our planet. The question is, how deep do such changes penetrate? Certainly shallow hydrothermal systems, including those involved in ore formation, have been involved in the change. Whether the lower crust or mantle see any of the surface effects remains to be studied. The concept of mineral evolution has yet to be fully explored, and if established,

Figure 8. Google Earth view of Pilbara craton, NW Australia. Eliptical areas of tan-gray TTG gneiss surrounded and divided by plunging keels of darker greenstone belts. Marble Bar is a little north of the center of this image. This image not only illustrates the unique tectonic style of the Archean craton's TTG/greenstone association, but also illustrates how information has become so very much more accessible in the past 50 years. Any school child with an internet connection can be an explorer on a scale undreamed of 50 years ago using these new digital tools.

Figure 2. The 2010 eruption of Eyjafjallajökull, Iceland, shut down many airports across Europe for over a week. Photograph taken on 17 April 2010 during the explosive phases that formed plumes of fine-grained volcanic ash that were swept across Europe. Photograph by Magnus Tumi Gudmundsson, Institute of Earth Sciences, Iceland.

is possible, and hundreds of calderas can be seen by scouring images on Google Earth™. Verbeek (1885) recognized Krakatau as a crater caused by collapse during the eruption of 1883. Studies of eroded volcanic fields in the British Isles concluded that subsidence occurred during large explosive volcanic eruptions. Within the United States, calderas were introduced into the geologic literature by Williams (1941) and study of Crater Lake in Oregon (Williams, 1942). The next major step took place following the studies of the Valles caldera in New Mexico by Smith and Bailey (1968). A proposed link between plutons and overlying calderas was developed mostly during studies of eroded plutonic-volcanic complexes such as those exposed in the Andes (Cobbing and Pitcher, 1972; Myers, 1975). Jacobson et al. (1958) interpreted the high-level ring-dike complexes of the Jos Plateau in Nigeria as the underpinnings of calderas. Since these earlier pioneering publications, what have been the major developments in understanding the origins of calderas?

The subject of calderas has not lost its appeal. In 1983 the celebration of the 100th anniversary of the Krakatau eruption involved a week-long session during the fall meeting of the American Geophysical Union (Lipman et al., 1984). Newhall and Dzurisin published their mammoth study *Historical Unrest at Large Calderas of the World* (1988). More recently the IAVCEI Commission on Collapse Calderas (http://www.gvb-csic.es/CCC.htm) has convened workshops at least every other year. *Caldera Volcanism: Analysis, Modeling and Response* (Gottsman and Martí, 2008) is an example of the Commission's integration of field observations, theory, and modeling in the laboratory.

Association of calderas with ignimbrites. Most calderas are flanked by widespread tephra deposits, which include Plinian pumice-fall deposits (not always), surge deposits, pyroclastic flow deposits (ignimbrites), and lithic clast concentrations within the ignimbrites. The pyroclastic flow deposits were deposited quickly (perhaps in days or weeks), can have enormous volumes, and, along with lithic clasts, supply information on the collapse process.

Scale. Many of the Earth's calderas were formed during the rapid eruption of tens to hundreds of cubic kilometers of pumice and ash. The La Garita caldera, one of the many overlapping calderas of the San Juan volcanic field, Colorado, comprises 35 × 75 km and is linked to the eruption of ~5000 km^3 of magma. Overlapping calderas at Yellowstone are up to 60 km in diameter and were formed during eruptions of 600 km^3 to 2000 km^3 of magma. Toba caldera in Sumatra is 30 × 80 km, which collapsed during an eruption of ~1500 km^3 of tephra. An especially influential leader in recognizing large calderas has been Peter Lipman, who, with many colleagues, has studied the many calderas of the San Juan volcanic field, southwestern Colorado, and elsewhere in the world.

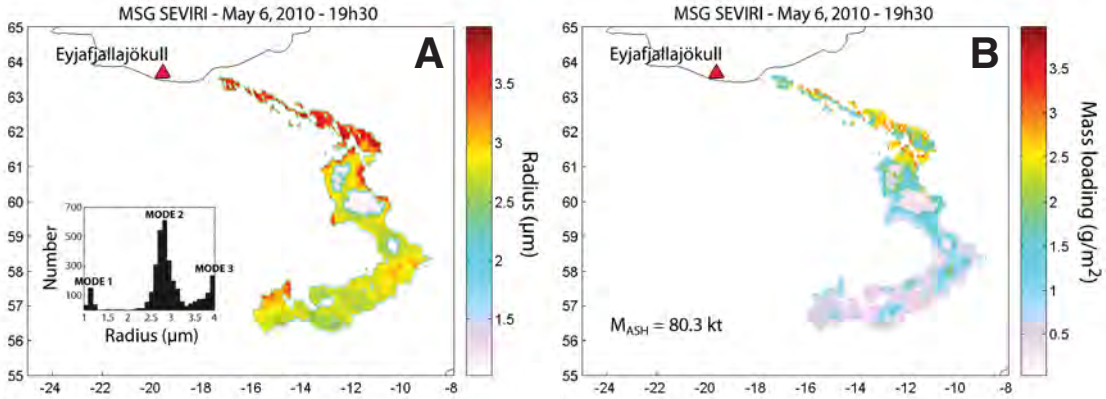

Figure 3. Detailed map of the Eyjafjallajökull ash plume on 6 May 2010 at 19:30 UT, created from data from the Meteosat Second Generation–Spinning Enhanced Visible and Infrared Imager (MSG-SEVIRI), showing (A) volcanic ash effective radii, with the corresponding particle size distribution displaying three main modes, and (B) ash mass loading inside the ash plume. From Bonadonna et al. (2011).

More recently it has become possible to try to investigate the relative effects of tectonic uplift versus geomorphic development. Using a restraining bend in the Carrizo Plain in California, Hilley and Arrowsmith (2008) documented the geomorphic evolution of a ridge (Dragon's Back) as it moved through a restraining bend. The authors were able to document that change in rock uplift rate occurred on the thousand year cycle, but hillslope processes took greater than an order of magnitude more time to adjust to uplift rates.

An underutilized approach is the documentation of microstructures along active geological structures. Cashman et al. (2007), for example, noted a difference in microstructures between the central creeping and locked segments of the San Andreas Fault. One problem is obtaining materials without the cost of trenching (or coring, in the case of the San Andreas Observatory at Depth; e.g., Zoback et al., 2011). Direct fault observation is commonly difficult for very young deformations, as only normal faults get self-exhumed. One spectacular example of fault exhumation is made available by the new shuttle imagery on newly forming extensional complexes (e.g., Daymon Dome, Papua New Guinea; Spencer, 2010). With the advent of ground-based LiDAR, structural geologists have also been documenting the detailed geometries of exposed fault surfaces. This information is also being obtained and utilized by scientists interested in the mechanics of earthquakes (e.g., Sagy et al., 2007; Brodsky et al., 2011).

The Seismic Cycle

Allmendinger et al. (2009) attempt to elucidate the links between geodetic information and finite strain measurements typically collected in studying ancient orogens. The difficulty is that the methods and time scales of geological and geodetic data largely do not overlap (Figs. 10, 13). A particular problem is that the seismic cycle (Fig. 13) is thought to dominate the geodetic signal. The "classic" seismic cycle (e.g., Reid, 1910; Fig. 13A) describes the time and deformation buildup between earthquake events; the only deformation that accumulates is elastic strain (Fig. 13A2), which is completely released when the earthquake occurs (Fig. 13A3). Many workers use models for seismic behavior that are built on this assumption and that utilize dislocation theory (e.g., Savage and Prescott, 1978; Savage, 1983). While there is no doubt that the dominant signal in the geodetic studies results from elastic strain buildup associated with the seismic cycle, some permanent non-recoverable strain occurs adjacent to large faults, which is inconsistent with the "classic" seismic cycle model (Fig. 13A). This permanent deformation is recorded using geodetic data (e.g., Hyndman and Wang, 1995) and fault formation (e.g., Loveless et al., 2009) in subduction-zone settings, distributed wrenching in strike-slip settings (e.g., Titus et al., 2007a), and modeled in analogue studies (Cooke et al., 2013). Thus, one can consider a "progressive"

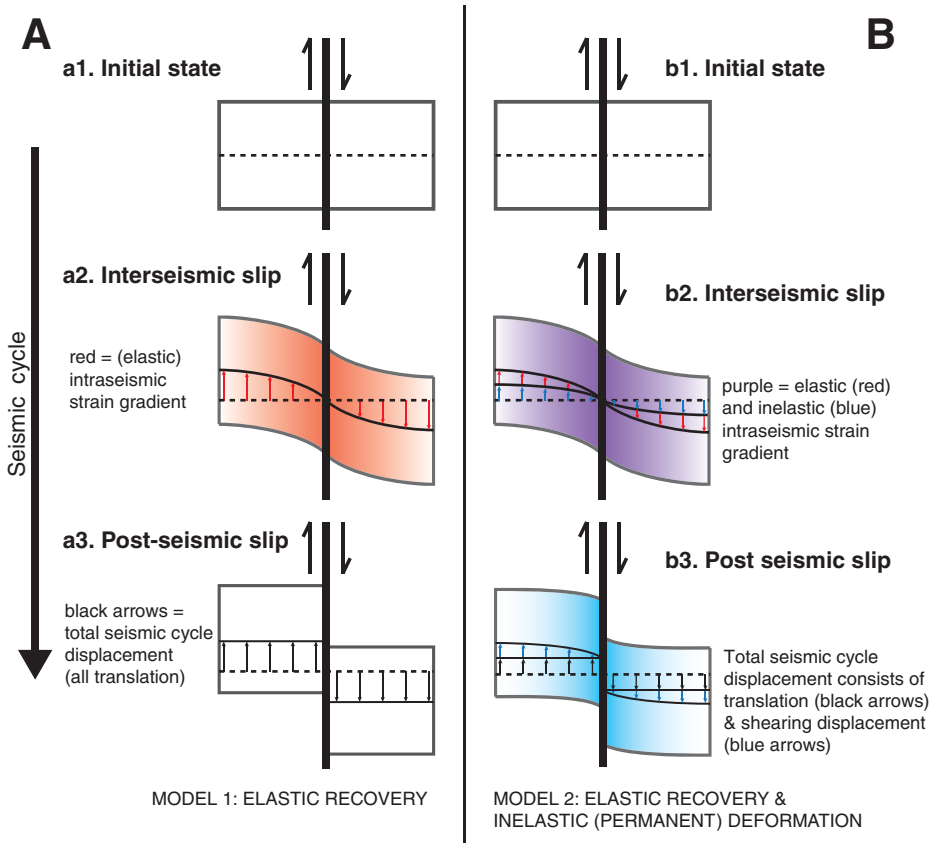

Figure 13. Two plots of the seismic cycle. (A) The "classic" seismic cycle, in which all the deformation adjacent to a major fault is elastic and is recovered at the end of the seismic cycle. Despite the fact that this model is incorrect, it is still the most commonly used. (B) A "progressive" seismic cycle, in which deformation adjacent to a major fault is a combination of recoverable (elastic) strain and permanent strain. The relative magnitudes of recoverable versus permanent strain is unknown, although the recoverable strain is likely >80%.

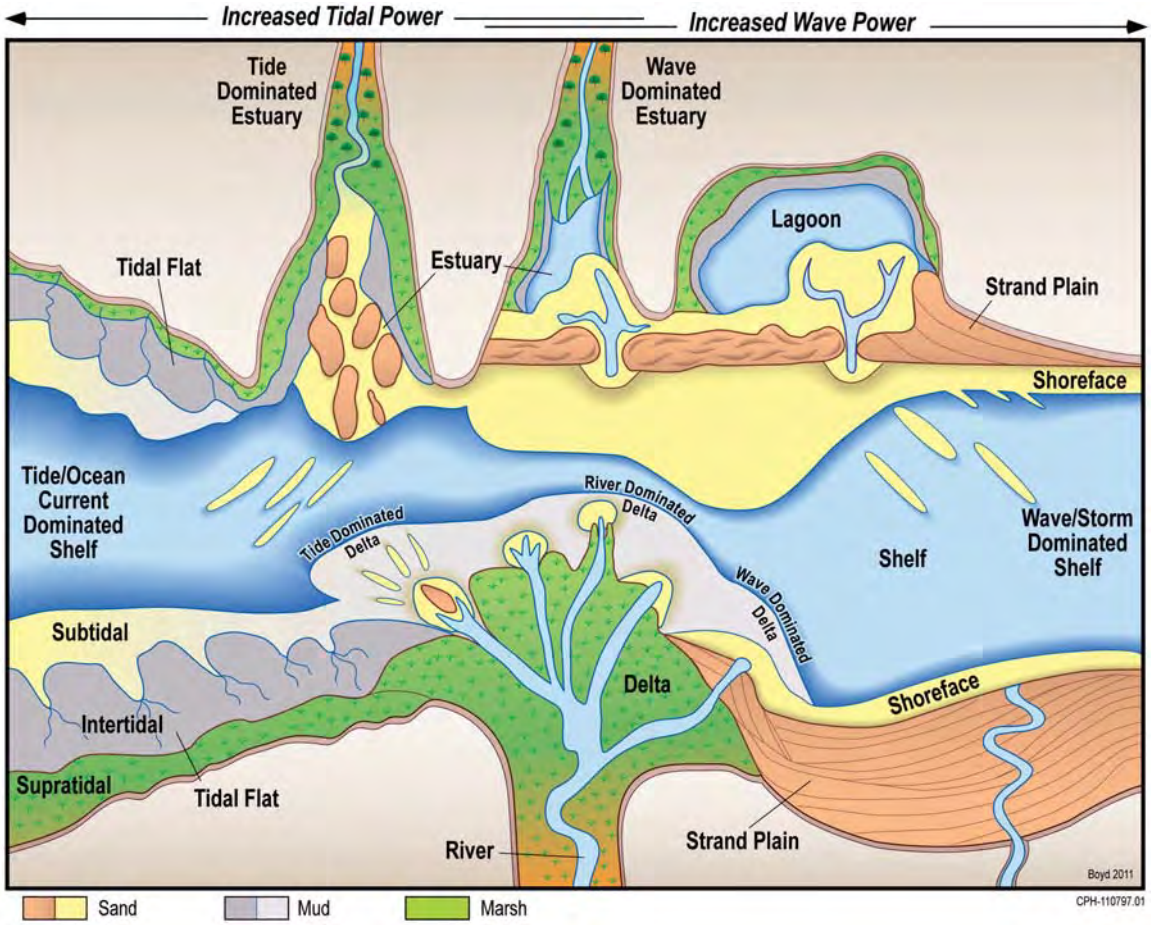

Figure 4. Range of common shallow-water depositional systems in a coastal classification based on ratio of wave power to tidal power (Boyd et al., 1992, with recent update in James and Dalrymple, 2010). The deltas, strand plains, and open-coast tidal flats (lower half of diagram) are regressive coastal environments, whereas estuaries, barrier-lagoon systems, and open coast tidal flats (upper half of diagram) are transgressive coastal environments. Shelf environments associate with both types of coast; shelf width increases during transgression and decreases during regression (diagram courtesy of Ron Boyd).

1980s: Delta instability, shelf-delta types, and sequence stratigraphy. The 1980s provided diverse research themes on deltas other than mainstream shelf deltas. Coarse-grained fan deltas became a popular topic, and these were explored as a distinct environment (McPherson et al., 1987; Colella et al., 1987; Nemec and Steel, 1988; Nemec, 1990). Deltas sited near the shelf-slope break, so-called *shelf-edge deltas* (though by this stage of the cross-shelf transit there is little or no remaining shelf in front of such deltas), were also highlighted, with their important linkage to shelf-edge and upper-slope instability and growth faults (Edwards, 1981; Winker and Edwards, 1983; Nemec et al., 1988) and their potential for dispersal of sandy sediment down to the deepwater parts of the basin (Suter and Berryhill, 1985). A third type of delta is the bayhead delta, at the landward side of the shelf, and there was an early account of the Atchafalaya Delta as a bayhead delta (Van Heerden and Roberts, 1988). A later publication (Porebski and Steel, 2006) shows how this entire delta family, from the shelf edge to the bayhead, varies in its geometry, thickness, and, to some extent, in its dominant process regime. Another related theme raised at this time, and mentioned further below, was the gigantic shore-attached banks of fluid mud derived from deltas such as the Amazon Delta (but stretching north to the Orinoco), described as nearshore, shore-parallel, prograding mud wedges, with mud suspended both by waves and tidal currents (Wells and Coleman, 1981).

By the late 1980s an important advance in our understanding of the evolution of delta lobes, building on the earlier ideas of Scruton (1960) and of Coleman and Gagliano (1964a, 1964b), came with the Mississippi work of Boyd and Penland (1988), Penland et al. (1988), and Boyd et al. (1989). They showed that a Mississippi delta lobe, over a period of 1–2 k.y., evolved from a progradational phase through abandonment and wave reworking into a barrier-lagoon system as the lobe compacts and sea level rises, and to an eventual sand shoal on the shelf. This lobe growth

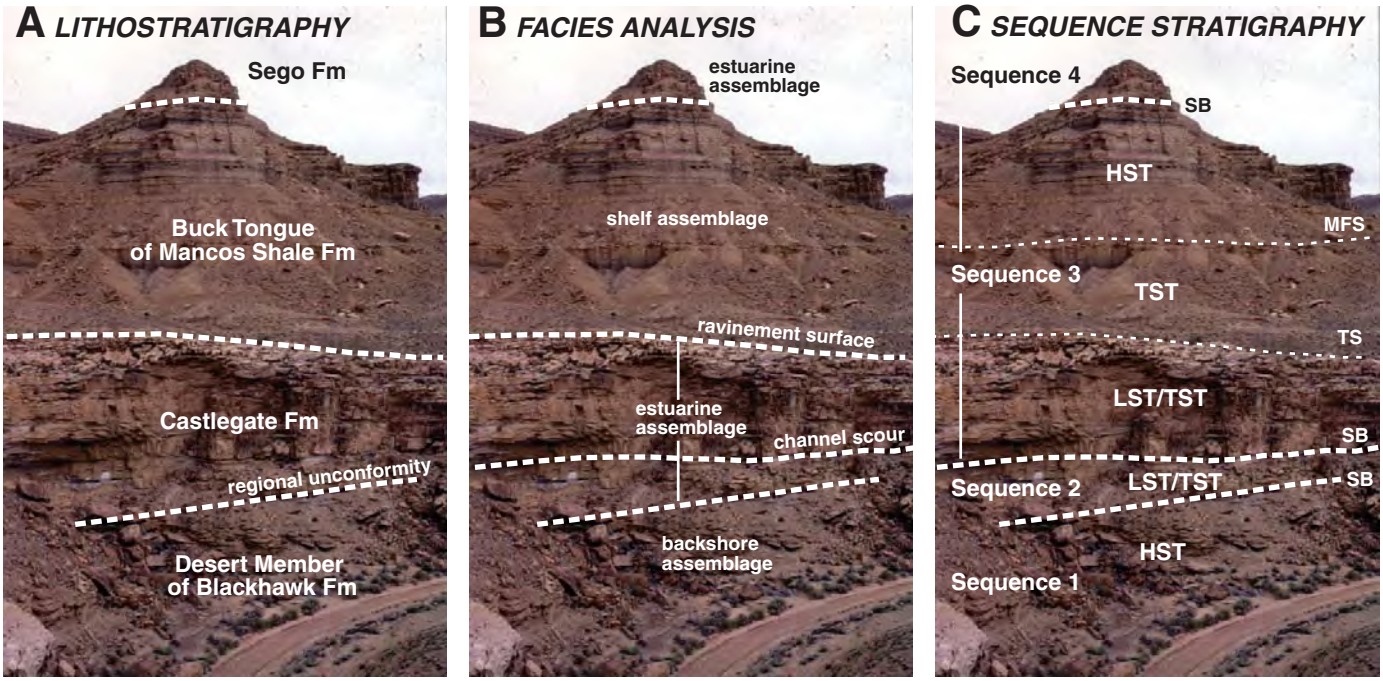

Figure 5. An outcrop in the Book Cliffs of Utah (Tusher Canyon, near Green River) interpreted using three successive deductive models of stratigraphic interpretation. (A) Lithostratigraphic terminology from the 1940s to 1960s. (B) Facies methods from the 1980s. (C) Sequence terminology, from the 1990s. Sequence-stratigraphic terminology: SB—sequence boundary, TS—transgressive surface, MFS—maximum flooding surface, LST, TST, HST—lowstand, transgressive and highstand systems tracts (from Miall, 2010).

sets (meters to tens of meters) has meant that, in practice, such reconstructions have been on a coarse scale. The advent of three-dimensional seismic methods has changed all that. The development of digital techniques and the acquisition of multiple, closely spaced vertical sections now permit data sets to be sampled in any direction. Horizontal (*seiscrop*) sections or, even better, those developed along specific stratal surfaces, eliminating any structural dip, can readily be generated. Because amplitude variations in the signal typically respond to lithology, by highlighting these subtle variations with the use of false colors, depositional systems can be revealed in their entirety. The methods were first described for use by petroleum geologists by A.R. Brown in 1986. This book is now in its sixth edition (Brown, 2004).

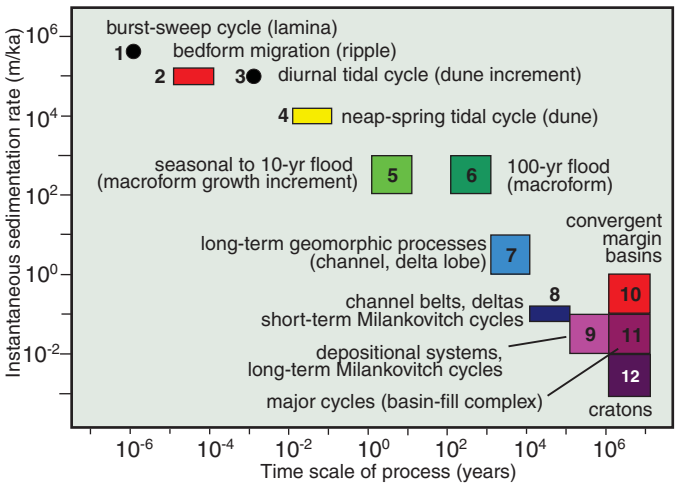

Figure 6. Rates and durations of sedimentary processes. Numerals refer to the Sedimentation Rate Scale (Miall, 2013).

The ability to "see" ancient depositional systems in the subsurface is of enormous value. Depositional features can be now mapped in detail and their evolution through time tracked from one time slice to the next. A new field of specialization, *seismic geomorphology*, has emerged, pioneered by Henry Posamentier (Davies et al., 2007). Spectacular reconstructions of complex three-dimensional objects deeply buried beneath later deposits can now be imaged, such as submarine fan-channels with their accompanying levee and overbank deposits, and buried karst surfaces cut by sink holes and subterranean drainages. Where the 3-D data can be used in combination with wireline log data and other records, such as down-hole pressures (which can be interpreted in terms of fluid connectivity between beds), such reconstructions can be made with enough precision that specific potential reservoir units can be targeted by directional drilling.

Much ingenuity has been employed to extend the range of techniques used to characterize and correlate sections in the subsurface. Mineralogical, petrological, and chemostratigraphic analyses have proved to be of particular use on a local to regional scale (e.g., Dunay and Hailwood, 1995; Ratcliffe and Zaitlin, 2010). Provenance studies, based on the dominant

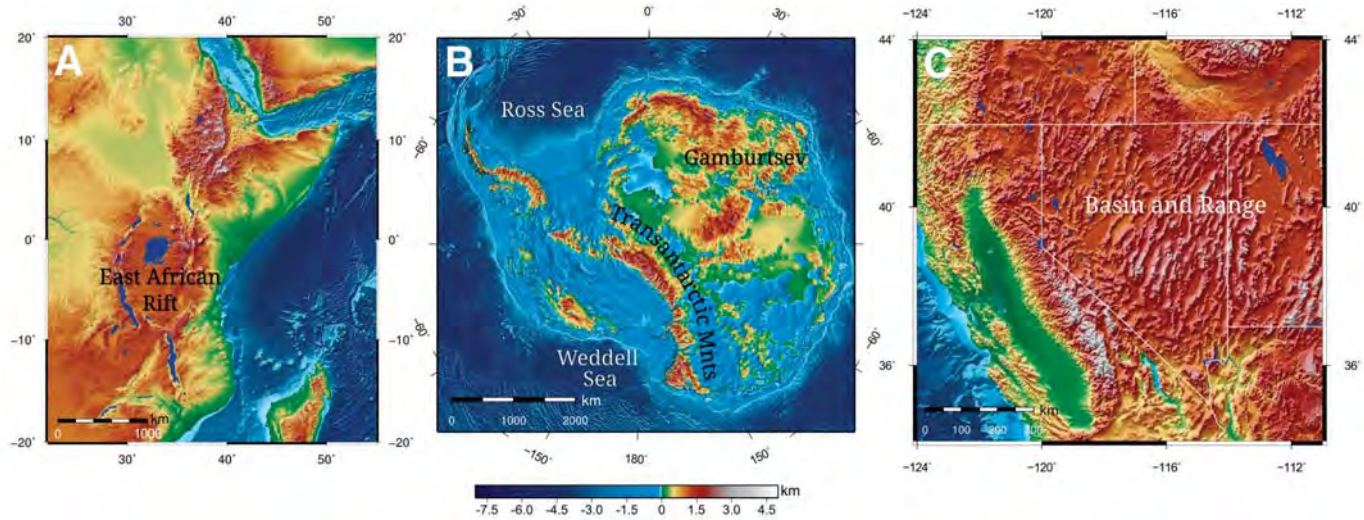

Figure 7. Digital elevation models of the world's major continental rifts, illustrating large elevation variations. (A) East African rift system, showing outline of Western and Eastern Rifts and relations to the Red Sea and the Gulf of Aden rift systems (modified after Burke, 1980). (B) Antarctic rifts: Ross Sea–Weddell Sea rift between West Antarctica (from Behrendt, 1991; Studinger et al., 2006, and www.ldeo.columbia.edu/~mstuding/tam_map_large.html) and the Gamburtsev Mountain rift system (after Ferraciolli et al., 2011). (C) Basin and Range Province, western North America, modified after Stewart (1978). Note large elevation contrasts and differences in scale. Elevation models after Amante and Eakins (2009).

to have a pronounced axial valley with isolated volcanoes and exposures of serpentinized peridotite. Detachment faults are present along many slow-spreading ridges (e.g., Karson, 1998; Tucholke, and Lin, 1994); see Figure 8. Fast-spreading ridge surfaces are smooth, with little or no normal faulting. Intermediate-spreading ridges show topography intermediate between the two end members.

For some very slow spreading-rate, magma-starved ridges, there is no magmatic crust at all, and the oceanic crust is made up of serpentinized peridotite, as originally proposed by Hess, (1962; see Fig. 2). In many cases the serpentinite appears to be the lower plate of a detachment fault, with pronounced "megamullions," ridges oriented parallel to the spreading direction (Tucholke et al., 1998, Blackman et al., 2002).

All ridges display deflections at transform fault intersections, as discussed below. Magma intrusion-extrusion tends to overlap with tectonic rifting, resulting in a varying amount of mixture of magmatic and faulting features.

Direct observations of oceanic crust (Karson, 2002) at three separate windows, the Hess Deep Rift (HD), a hole through fast-spreading crust that formed the Galapagos Rift; the Blanco Transform escarpment, an exposure of intermediate-rate spreading along the Juan de Fuca Rift; and the Pito Deep (Hayman and Karson, 2009), an exposure in the small Easter microplate

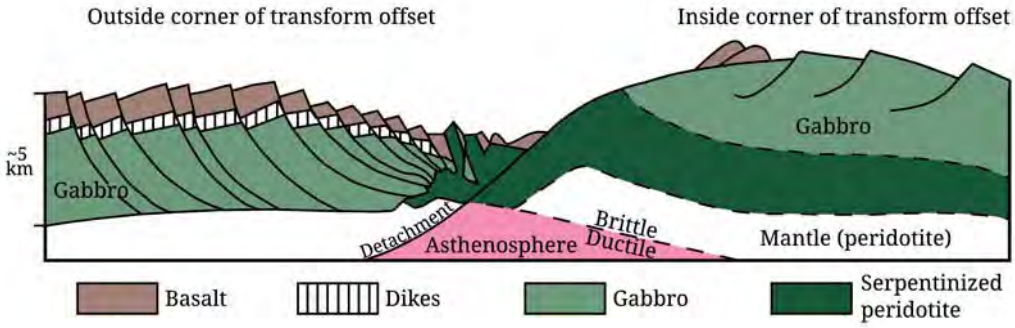

Figure 8. Example of asymmetric spreading along a slow-spreading ridge. Schematic cross section of a faulted ridge near a transform fault zone, with a complete crustal sequence on the left, flanked by an eroded sequence on the right. Sequence on the left (outside corner) represents a corner near an inactive fracture zone; the sequence on the right represents a section near an inside corner, bordering the active transform fault. Zones of serpentinization of mantle peridotite are shown schematically. Redrawn after Lagabrielle et al. (1998) and Twiss and Moores (2007, fig. 19.16, p. 594).

the sub-lacustrine Tanganyika earthquakes is available to compare with the empirical fault-length displacement ratios. Independent data from the Malawi rift zone show that entire 100-km-long fault segments can rupture in single or coupled earthquake events (e.g., Jackson and Blenkinsop, 1997).

5. EPISODIC RIFTING ON THE MILLIONS OF YEARS TIME SCALE: OBSERVATIONS FROM THE RIO GRANDE RIFT

The Rio Grande rift zone extends over a distance of >1000 km from Leadville, Colorado, to Chihuahua, Mexico (Fig. 7). The northern part of the rift separates the Colorado Plateau on the west from the Great Plains on the east. It consists of a series of narrow rift basins trending approximately N-S. These basins resulted from a recent late Miocene–Holocene extensional phase (Morgan et al., 1986). An early event of crustal extension occurred during middle Oligocene–early Miocene time. Basins formed during this extensional phase were much broader than the younger basins (Baldridge et al., 1994), and they trended northwestward in contrast to the young N-S basins. The exact age of initiation of extension for the Rio Grande rift is debated. If the oldest erupted basalts and silicic volcanic rocks are taken as an indication for the onset of extension, then extension is estimated to have started in the Oligocene (Ingersoll, 2001). The earliest rift-related sedimentary rocks have younger ages, however, ranging from late Oligocene to early Miocene (Keller and Cather, 1994; Ingersoll, 2001).

The Rio Grande rift has not been widening significantly in historic times. GPS measurements suggest a current opening rate of ~1 mm/yr (Savage et al., 1980; Berglund et al., 2012). Large Holocene earthquakes have been documented to occur on several of its border faults, however, including the Pajarito fault of the Española Basin. Here, a Holocene earthquake occurred as recently as ca. 1.5 ka, and many other large Holocene earthquakes have been documented along the rift (McCalpin, 2005; Section 6). Such observations from currently active rifts point toward an episodic pattern of continental rifting: Rifts are actively widening and lengthening during short (magmatic and/or fault controlled) events, followed by a phase of relative quiescence.

Rifting in the Rio Grande rift region has been episodic on the millions-of-years time scale, with separate rifting events from the late Cenozoic to the Quaternary. Rifting has been described as being multi-phased (Morgan et al., 1986; Ingersoll, 2001; Smith et al., 2002); a first period of extension occurred from ca. 27–20 Ma, and a second period occurred beginning at 10 Ma until recent times. Magmatic activity reflects the episodic rift behavior; the time in between the rapid rifting phases was characterized by minimal magmatism (Morgan et al., 1986; Baldridge et al., 1991). A compilation of igneous rock ages from New Mexico

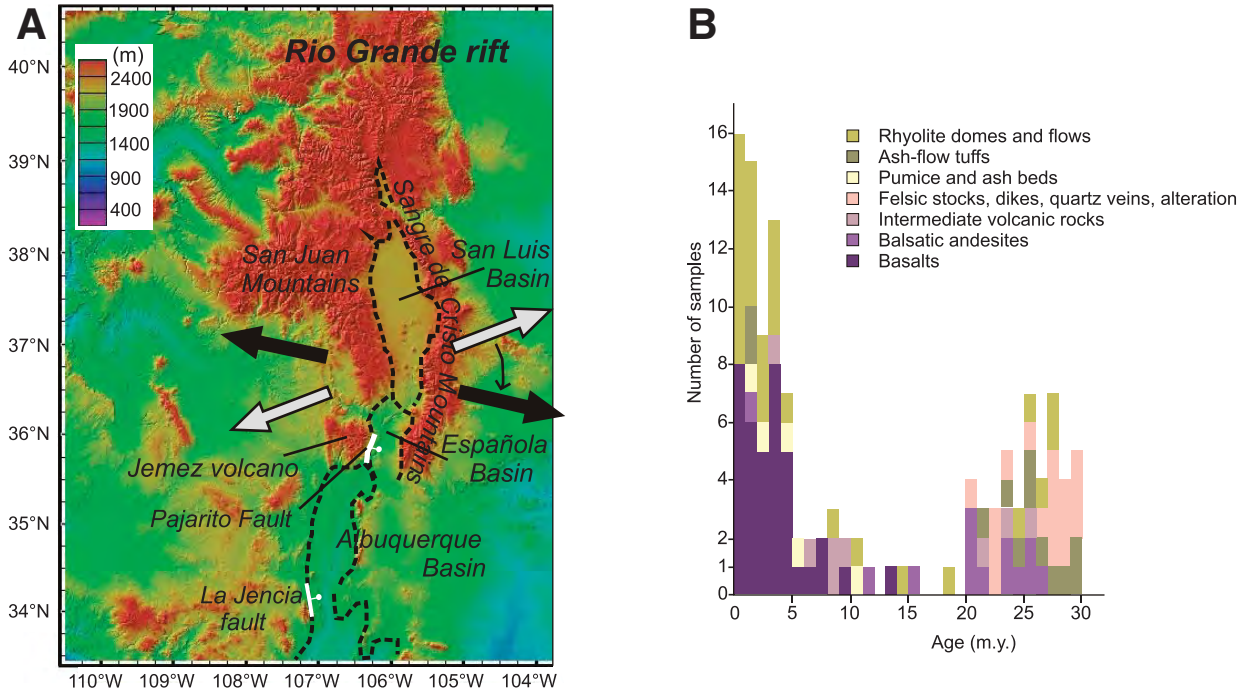

Figure 7. (A) N-S–oriented Neogene basins of the northern Rio Grande rift (outlined by dashed lines), Pajarito and La Jencia normal faults (see text for discussion), indicated by white lines, and least principle stress directions from Zoback et al. (1981). Paleo-stress field indicated by white arrows, recent stress field indicated by black arrows. (B) Histogram of igneous rock ages from Oligocene present in New Mexico from Chapin and Seager (1975). The period of tectonic quiescence in the Rio Grande rift (estimated between ca. 20 and 10 Ma) coincides with a period of lesser igneous activity in New Mexico. Ages based on K/Ar and fission track dates.

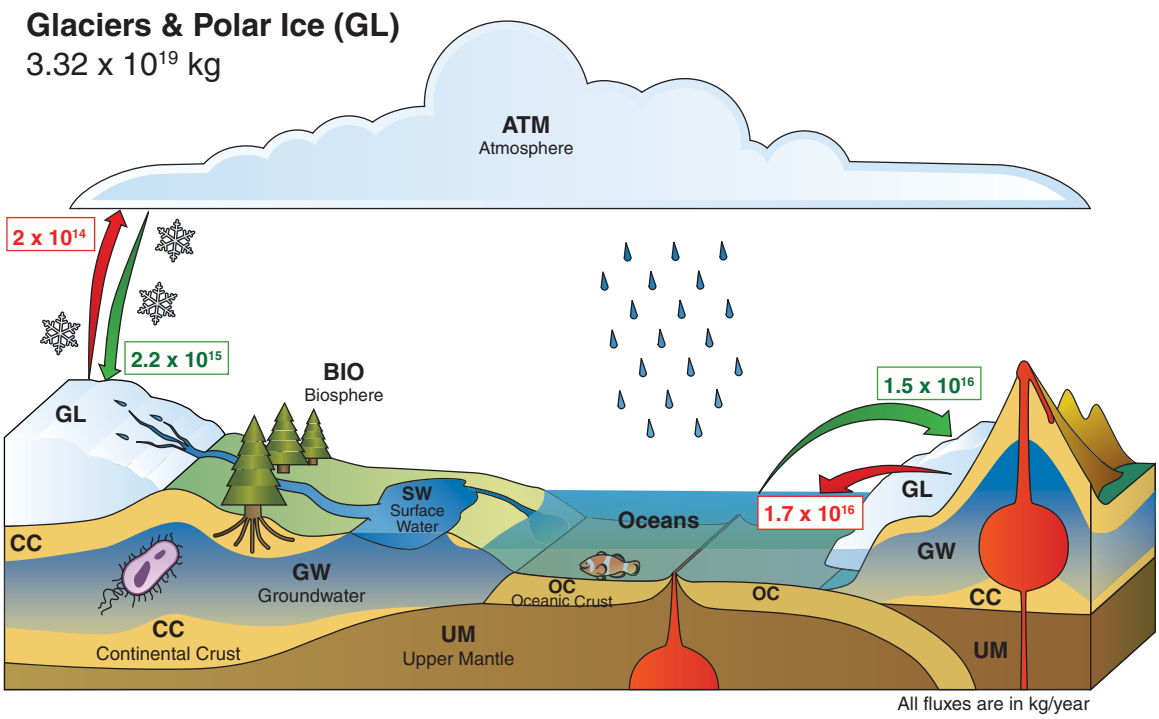

Figure 8. Summary of the fluxes of water between glaciers and polar ice (GL) and other reservoirs within the geohydrologic cycle. Green arrows represent fluxes into the reservoir, and red arrows represent fluxes out of the reservoir. All fluxes are in kg/yr.

750 × 10^{12} kg of dry heterotrophic biomass (300 / 0.4) × 10^{12} kg). Finally, the 800 × 10^{12} kg of C in all biomass (phytomass + heterotrophic biomass) correspond to (800 / 0.4) × 10^{12} kg of biomass, or 2000 × 10^{12} kg (2 × 10^{15} kg) of dry biomass.

Most organisms are dominantly H_2O, ranging from ~60% by weight in humans and other mammals, to over 90% in some fruits and vegetables such as tomatoes (95%) and watermelons (92%). On average, ~70% of biomass weight is H_2O. Thus, 2 × 10^{15} kg of dry biomass correspond to 6.7 × 10^{15} kg of "wet" or hydrated biomass. Accordingly, the amount of H_2O contained in the Earth's biosphere is estimated to be 4.7 × 10^{15} kg (Fig. 9; Tables 1, 2). This is ~4 times the amount of H_2O in the biosphere reported by Gleick (1996), which is the amount that is commonly used by other workers. Note, however, that these earlier estimates ignore the recently recognized deep subsurface biosphere.

Of the total amount of H_2O in the biosphere, 62.5% is contained in phytomass—this equates to 2.9 × 10^{15} kg of H_2O, and was obtained by taking the amount of dry phytomass given above (1250 × 10^{12} kg) and assuming that this represents 30% of the mass of hydrated phytomass. Subtracting the dry mass (1250 × 10^{15} kg) from this total gives the amount of water in the phytomass component of the biosphere. The remaining H_2O (37.5%, or ~1.75 × 10^{15} kg) is contained in heterotrophic biomass, dominantly in prokaryotes. This amount was estimated following the same procedure as described above for phytomass. Of this amount, we assume that 5% of the total biomass H_2O (= 0.24 × 10^{15} kg) is contained in soil and rock above the water table, and 32.5% of the total biomass H_2O (= 1.51 × 10^{15} kg) is contained in soil and rock beneath the water table. There are few data to justify or test this distribution of biomass, other than the fact that a much larger volume of subsurface biosphere occurs below, rather than above, the water table, and this distinction is necessary to estimate fluxes between the biosphere and other reservoirs.

Groundwater

Groundwater is pore water and water in fractures in the Earth's crust. In order to quantify the amount of water contained in the groundwater reservoir, it is first necessary to define the physical limits of the reservoir. The top of the groundwater reservoir is easily defined as the water table, but the bottom is less well defined. Water and brines have been documented at depths approaching 10 km in sedimentary basins during oil and gas exploration and production (Takach et al., 1987), and deep scientific drilling has encountered open fractures with water at 8–12 km in the Kola Superdeep SG-3 borehole in Russia (Zharikov et al., 2003) and at ~7 km in the KTB hole in Germany (Erzinger and Stober, 2005).

One possible choice for the bottom of the groundwater reservoir might be the brittle-ductile transition (Ingebritsen et al., 2006). At depths greater than this, interconnected fractures are unlikely to be present. However, the brittle-ductile transition does not occur at a fixed depth but, rather, varies as a function of lithology, geothermal gradient, and strain environment. Thus, quantifying the volume of the brittle portion of the system is

All organisms can leave an imprint on the environment, and vice versa. However, more often than not, geobiologic study tends toward investigating the role of microorganisms in the Earth system. This is not to say that "macrobes" (e.g., animals, plants, etc.) are excluded from geobiologic investigation, but in general, microbes are omnipresent on Earth and are responsible for cycling most if not all of the bioessential elements in the Earth system, as well as other Earth important processes (e.g., weathering–mineral dissolution–precipitation, etc.). Furthermore, as we will discuss, molecular biologic techniques have opened up the study of microbes in the environment in a way not possible in the past.

Geology and a Map of Time

The field of geology has studied and divided Earth's history into a series of geologic eons, eras, periods, and epochs that are well defined based on observed processes after examination of the rock record of the Earth. A basic chronology with "life processes" superimposed on geologic processes is afforded by DesMarais, Konhauser, and others (DesMarais, 2000; Konhauser, 2007) (Fig. 1). As depicted in Figure 1, the origin of the Earth occurred ~4.6 billion years (Ga) ago. What followed was a late heavy bombardment to 4 Ga, and speculation abounds that life likely arose shortly thereafter, perhaps at 3.8 Ga. Geologists long ago realized that the history and story of Earth is best told through the rock record. Geologic time is on a grand scale, almost imperceptible, with time measured in billions of years. Geologists have been able to employ various dating schemes to pinpoint Earth's processes across that time.

With decades of both great field- and laboratory-based geology, the science of geology has greatly advanced what is known of the Earth, and what is known of the life on Earth. Many time points are hugely significant across the time of Earth's existence (Fig. 1); the advent of photosynthesis, ca. 3.8 Ga; an oxygenated atmosphere at ca. 2.4 Ga, microbiologically created, that arose after a long period of a reducing atmosphere; a "snowball Earth" at ca. 2.3 Ga and ca. 730–635 Ma; the Cambrian explosion of ca. 540 Ma with the first abundant fossils of macrobial life; the first vertebrate land animals at ca. 360 Ma; the Permian–Triassic extinction at ca. 250 Ma that is thought to have killed >90% of all marine invertebrates; the Cretaceous–Paleogene extinction at ca. 65 Ma that is thought to have killed off the terrestrial dinosaurs; the first appearance of hominids at ca. 7 Ma; the first appearance of *Australopithecus* at ca. 3.9 Ma, an ancestor of humans, *Homo sapiens;* to 200,000 years ago, the first modern *Homo sapiens,* humans' direct ancestor, who appeared in East Africa.

Life arose early, on the bacterial line of descent, and likely shortly after the late heavy bombardment (Pace, 1997). From 3.8 to 2.5 Ga, microbial life arose with remarkable sophistication,

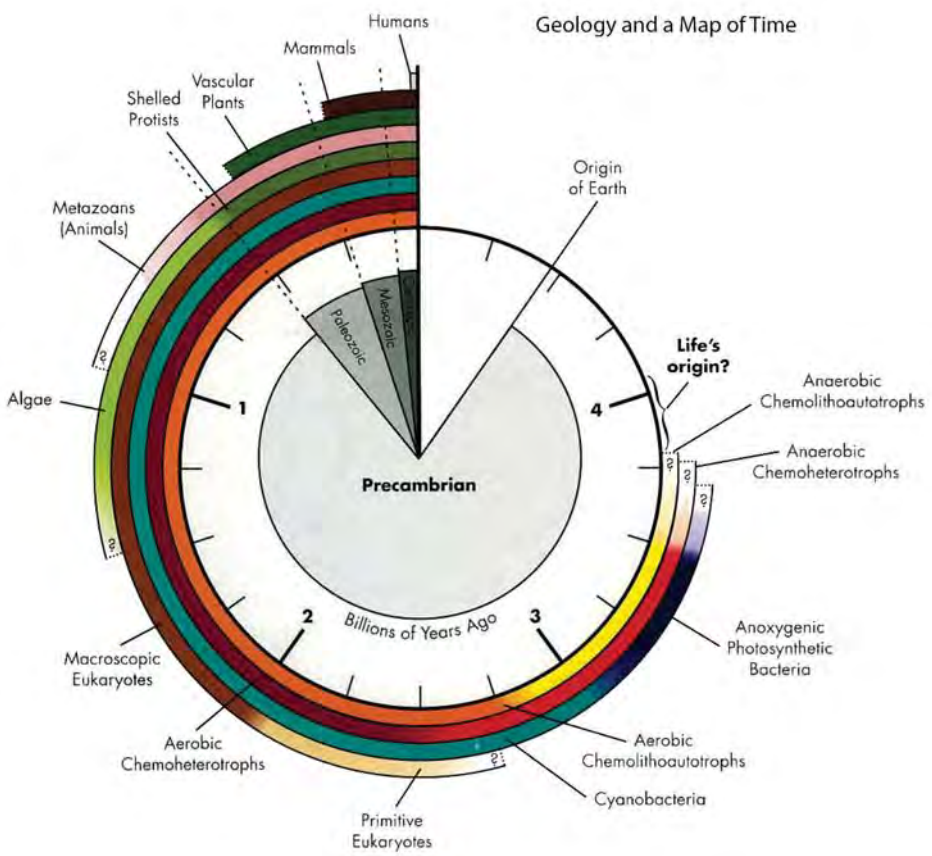

Figure 1. A biogeologic clock, as adapted from DesMarais (2000) and Konhauser (2007).

Figure 2. Sedimentary environments favorable for capturing and preserving biosignatures. (A) Aerial view of Laguna Ojo De Libre, a hypersaline lagoon on the Vizcaino Peninsula of Baja Sur, Mexico. (Image credit: Jack Farmer.) (B) Gypsum deposits adjacent to Laguna Ojo de Libre, which have precipitated from brine ponds at Exportadora del Sol, Guerrero Negro, Baja Sur, Mexico. Brownish areas are gypsum, while the white areas are halite. The image is ~0.5 m wide. (Image credit: Jack Farmer.) (C) Grand Prismatic Spring, Yellowstone National Park, Wyoming. This is the largest hot spring in North America. Colors indicate the presence of cyanobacterial communities, which are arrayed along outflow channels according to their temperature tolerances. (D) Mid-temperature pond at Fountain Paint Pots in the Lower Geyser Basin of Yellowstone National Park shows in situ fossilization of microbial mats owing to encrustation by silica. Darker areas at the top of the image are ponded hydrothermal waters (~55 °C) with actively growing microbial mats. White areas in the foreground are areas where spring flows have ceased, exposing light-toned silicified microbial mats and columnar microbialites. (E) Fossilized cyanobacteria preserved in gypsum from Miocene sulfate evaporite deposits in northern Italy (see Schopf et al., 2012, for details). (F) Silica-coated cyanobacteria from low temperature (<35 °C) distal apron facies at Fountain Paint Pots, Lower Geyser Basin, Yellowstone National Park, Wyoming. (Image credits: A–D and F are by Jack Farmer; Image E is reproduced from Schopf et al., 2012.)

ongoing supply of organic compounds endogenously, or recycled from the surface of the moon.

As with Mars, evidence for hydrothermal circulation may aid the exploration for life. Where water has welled up from the subsurface on Europa, it may have carried microorganisms, or their by-products, from an underlying ocean, or interstitial brine, freezing and cryopreserving these materials in ices at or near the surface (Sagan, 1971). But what are the chances that life could survive, once entombed and frozen in ice? Long-term survival in a frozen state is suggested by the revival of microbes from permafrost soils on Earth dated at ca. 3.0 Ma (Gilichinsky, 1995). However, in the absence of active DNA repair mechanisms, the long-term viability of microorganisms in ice has been questioned on the basis of the destructive effects of prolonged exposure to background radiation (see Kennedy et al., 1994). The radiation-rich environment of Europa could certainly pose a problem for the long-term survival of organisms in near-surface ices, and could degrade any complex organic compounds present. But viability arguments aside, ice could still be an important environment for cryopreservation of a fossil record of residual organic matter on Europa (Farmer and Des Marais, 1999), particularly at depths exceeding the penetration of destructive surface radiation. In exploring for a europan "cryopaleontology," landing sites where water-ice has recently erupted at the surface would have obvious priority (e.g., Gilichinsky et al., 1993; Figueredo et al., 2003).

The Cassini-Huygens encounter with Titan, the moon of Saturn (Fig. 8A), has forced us to widen our views of what may constitute a habitable environment in the Solar System, forcing a more universal approach to exploration than simply to "follow the water." As the primary solvent for life processes, water has provided an understandable focus for astrobiological exploration of the Solar System. It is good to build on what you know! But the discovery of geomorphic features (stream beds and shorelines) on Titan, apparently carved by a mixture of liquid methane and water (Mitri et al., 2007), has taken the discussion of habitability in new directions, along with the discovery of extensive hydrocarbon lakes on the surface (Fig. 8B; Stofan et al., 2007). While foreign to terrestrial experience, the potential of liquid hydrocarbons (e.g., methane and ethane) to act as alternative solvents for life has received wide discussion (NRC, 2007; Plaxco and Gross, 2006; McKay and Smith, 2005; Bains, 2004; Benner et al., 2004; Sagan and Dermott, 1982). In the absence of compelling terrestrial analogues, the concept of alternative solvents for life has remained within the realm of speculation. However, we cannot dismiss the possibility that life could have arisen on a different basis, following unique, non-terrestrial evolutionary pathways. This challenges our terracentric views in defining life, and encourages more universal approaches, including new technologies for future life detection missions for these extreme environments.

SUMMARY

Recent scientific advances have greatly expanded our knowledge of the nature and evolution of terrestrial life, while opening up new possibilities for the existence of extraterrestrial life. These developments have laid the foundation for a new interdisciplinary scientific discipline, astrobiology, which studies the origin, evolution, distribution, and destiny of life in the Cosmos. Geobiology is a core discipline of astrobiology, which has fostered important, new transdisciplinary approaches for discovering past or present habitable environments for life elsewhere in the Solar System, or beyond.

Advances in molecular biology and paleontology have revealed that Earth's biodiversity is predominantly microbial and that this has been the case for all of Earth's history. Over this period, microbiological processes have contributed extensively to biogeochemical cycles and have helped to shape the global planetary environment. Evolutionary pathways followed by the biosphere have been largely opportunistic, although ultimately tied to the inorganic processes of planetary evolution. However, some

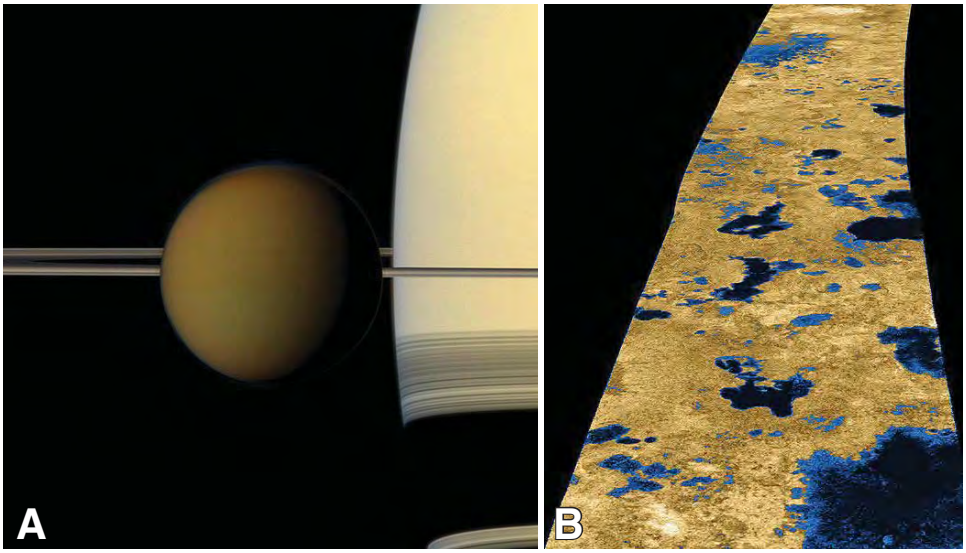

Figure 8. Hydrocarbon seas and lakes on Titan, a moon of Saturn. (A) Titan, in its orbit around Jupiter. This moon has a radius of ~2578 km. The surface is obscured by a dense, hydrocarbon-rich atmosphere. (B) Acquired in 2006, this Cassini spacecraft radar image shows the distribution of liquid hydrocarbon lakes in the north polar region of the moon. The lakes are thought to consist predominantly of methane-ethane, a possible solvent for alternative forms of life. (Image credits: NASA/ESA.)